ELSEVIER

Journal of Alloys and Compounds 388 (2005) 126–137

Journal of ALLOYS AND COMPOUNDS

www.elsevier.com/locate/jallcom

The influence of thermal treatment on the phase development in HfO_2–Al_2O_3 and ZrO_2–Al_2O_3 systems

G. Štefanić*, S. Musić, R. Trojko

Ruđer Bošković Institute, P.O. Box 180, HR-10002 Zagreb, Croatia

Received 10 May 2004; received in revised form 13 July 2004; accepted 13 July 2004

Abstract

Amorphous precursors of HfO_2–$AlO_{1.5}$ and ZrO_2–$AlO_{1.5}$ systems covering the whole concentration range were co-precipitated from aqueous solutions of the corresponding salts. The thermal behaviour of the amorphous precursors was examined by differential thermal analysis, X-ray powder diffraction (XRD), laser Raman spectroscopy and scanning electron microscopy. The crystallization temperature of both systems increased with increase in the $AlO_{1.5}$ content, from 530 to 940 °C in the HfO_2–$AlO_{1.5}$ system, and from 405 to 915 °C in the ZrO_2–$AlO_{1.5}$ system. The results of phase analysis indicate an extended capability for the incorporation of Al^{3+} ions in the metastable HfO_2- and ZrO_2-type solid solutions obtained after crystallization of amorphous co-gels. Precise determination of lattice parameters, performed using whole-powder-pattern decomposition method, showed that the axial ratio c_f/a_f in the ZrO_2- and HfO_2-type solid solutions with 10 mol% or more of Al^{3+} approach 1. The tetragonal symmetry of these samples, as determined by laser Raman spectroscopy, was attributed to the displacement of the oxygen sublattice from the ideal fluorite positions. It was found that the lattice parameters of the ZrO_2-type solid solutions decreased with increasing Al^{3+} content up to ~10 mol%, whereas above 10 mol%, further increase of the Al^{3+} content has very small influence on the unit-cell volume of both HfO_2- and ZrO_2-type solid solutions. The reason for such behaviour was discussed. The solubility of Hf^{4+} and Zr^{4+} ions in the aluminium oxides lattice appeared to be negligible.

Keywords: ZrO_2–$AlO_{1.5}$; HfO_2–$AlO_{1.5}$; XRD; Raman spectroscopy; DTA; SEM/EDX

1. Introduction

Pure hafnia and zirconia exhibit similar physical and chemical properties, which made them very interesting high-temperature materials. In dependence on the temperature, HfO_2 and ZrO_2 appear as monoclinic (*m*-HfO_2, *m*-ZrO_2), tetragonal (*t*-HfO_2, *t*-ZrO_2) and cubic (*c*-HfO_2, *c*-ZrO_2) polymorphs of which only the monoclinic is thermodynamically stable at RT and standard pressure. High temperature polymorphs of ZrO_2 become stable at above 1170 °C (*t*-ZrO_2) and 2300 °C (*c*-ZrO_2), whereas the stabilization of *t*- and *c*-HfO_2 require significantly higher temperatures, 1720 and 2600 °C, respectively. Metastable *t*-ZrO_2 can be easily obtained at RT as a product of the thermal decomposition of zirconium salts [1,2] or as the crystallization product of hydrous zirconia [3]. In the case of hafnia, the formation of metastable *t*- or *c*-HfO_2 (ratio *c*/*a* is nearly 1) at RT is much harder to obtain [4–8]. Cubic polymorphs of HfO_2 and ZrO_2 can be stabilized at RT by the incorporation of aliovalent oversized metal cations, viz. Ca^{2+}, Sc^{3+}, Y^{3+}, etc. [9–17]. Stabilization of these high-temperature polymorphs was attributed to the decrease in the Hf and Zr coordination number caused by the introduction of oxygen vacancies [2,9,17].

The incorporation of aliovalent undersized dopant cations, such as Al^{3+}, Fe^{3+} or Cr^{3+}, also introduces oxygen vacancies into the HfO_2 and ZrO_2 lattice. However, in the thermodynamically stable systems the amount of the incorporated dopants is too small to stabilize their high-temperature polymorphs [17–20]. The results of phase analysis of the ZrO_2–$CrO_{1.5}$ system showed that, regardless of the negligible solubility of the Cr^{3+} ions, partial stabilization of a

* Corresponding author. Tel.: +385-1-456-1111; fax: +385-1-46-80098.
E-mail address: stefanic@rudjer.irb.hr (G. Štefanić).

0925-8388/$ – see front matter © 2004 Elsevier B.V. All rights reserved.
doi:10.1016/j.jallcom.2004.07.004

metastable t-ZrO_2 occurred [20]. The observed stabilization was attributed to surface interaction between Cr_2O_3 and ZrO_2. This interaction prevented the diffusion of oxygen from the atmosphere into the ZrO_2 lattice, which otherwise triggered the transformation t-$ZrO_2 \rightarrow m$-ZrO_2 on cooling [20].

The solubility of undersized dopant cations in the metastable HfO_2- and ZrO_2-type solid solutions obtained after crystallization of amorphous precursors is significantly higher. High temperature cubic and tetragonal polymorphs of HfO_2 and ZrO_2 could appear in such metastable solid solutions. However, such stabilization is not very efficient [7,8,21–24]. In our previous investigations, we examined the thermal behaviour of the amorphous precursors to the HfO_2–$FeO_{1.5}$ and ZrO_2–$FeO_{1.5}$ systems [7,8,24]. It was found that the incorporation of Fe^{3+} ions has both a stabilizing and destabilizing influence on the high-temperature polymorphs of HfO_2 and ZrO_2. The destabilizing influence significantly increased if the thermal treatments were performed at small air pressure ($\sim 4 \times 10^{-3}$ Pa), which was attributed to the association of the introduced oxygen vacancies with smaller Fe^{3+}cations [7,8].

The capability of Al^{3+} ions to stabilize the cubic polymorph of zirconia in the metastable solid solutions is still a matter of discussion [25–35]. Several authors reported that the amorphous precursors to the ZrO_2–Al_2O_3 system crystallized after heating between 500 and 900 °C to c-ZrO_2-type solid solution containing up to 40 mol% Al_2O_3 [25–29]. At higher temperature c-ZrO_2 converted to t-ZrO_2 and finally to m-ZrO_2 that was followed by a decrease in Al_2O_3 solubility. On the other hand, other reports [31–35] stated that the incorporation of Al^{3+} ions into the ZrO_2 lattice stabilized only the tetragonal polymorph of zirconia.

Differently from the ZrO_2–$AlO_{1.5}$ system, the stabilizing influence of Al^{3+} ions in the HfO_2–$AlO_{1.5}$ system was much less investigated. In the present work, we focused on the thermal behaviour of the amorphous precursors to the HfO_2–$AlO_{1.5}$ and ZrO_2–$AlO_{1.5}$ systems, covering the whole concentration region. The capability of Al^{3+} ions to incorporate into the HfO_2 and ZrO_2 lattice and stabilize their high-temperature polymorphs was discussed.

2. Experimental

Amorphous precursors of the HfO_2–$AlO_{1.5}$ (HA) and ZrO_2–$AlO_{1.5}$ (ZA) systems covering the whole concentration range were co-precipitated from aqueous solutions of $HfOCl_2 \cdot 8H_2O$ and $AlCl_3 \cdot 6H_2O$ salts and aqueous solutions of the $ZrO(NO_3)_2 \cdot 2H_2O$ and $Al(NO_3)_3 \cdot 9H_2O$ salts, respectively. The co-precipitations were performed by the addition of 25% NH_3·aq. up to pH ~7.5. All the chemicals used were of analytical grade. The solid phase was separated from the liquid using an ultra-speed centrifuge (operational speed up to 20,000 rpm), then washed repeatedly in doubly distilled water and dried at 70 °C for 24 h. The obtained solid phases were ground in an agate mortar and calcined for 3 h at the selected temperatures up to 1300 °C. The phase compositions of the obtained crystallization products were analysed at RT using X-ray powder diffraction (XRD). XRD patterns were recorded using an automated Philips diffractometer (model MPD 1880) with monochromatized Cu Kα radiation. Silicon, α-Si, was used as internal standard (space group $Fd\bar{3}m$, unit-cell parameter at 25 °C: a = 5.43088 Å, [36]). XRD patterns were scanned in steps of 0.03° (2θ), in the 2θ range from 20° to 110°, with a fixed counting time (5 or 10 s), for the purpose of the accurate determination of the unit-cell parameters of the studied samples by means of the powder-pattern-fitting methods.

In case where monoclinic and tetragonal polymorphs of hafnia or zirconia co-exist their volume fractions (ν_t and ν_m) were estimated from the integral intensities of the monoclinic diffraction lines $(\bar{1}\,1\,1)$ and $(1\,1\,1)$ and tetragonal diffraction line $(1\,0\,1)$, following a procedure proposed by Toraya et al. [37]. The volume fractions are given by following equations:

$$x = \frac{I_m(\bar{1}\,1\,1) + I_m(1\,1\,1)}{I_m(\bar{1}\,1\,1) + I_m(1\,1\,1) + I_t(1\,0\,1)}, \quad (1)$$

$$\nu_t = 1 - \nu_m, \quad (2)$$

$$\nu_m = \frac{1.311x}{1 + 0.311x}, \quad (3)$$

Integrated intensities of the diffraction lines were determined using the individual profile-fitting method (computer program PRO-FIT) [38].

Laser Raman (DILOR Z24) spectroscopy was also used in the cases when the presence of the cubic or tetragonal polymorphs of hafnia and zirconia could not be clearly distinguished by XRD.

The first crystallization products of some samples at the ZrO_2-rich side of the concentration range were also analysed with a scanning electron microscope (JSM-5800 JEOL) equipped with an energy dispersive X-ray spectrometer (LINK ISIS 300 Oxford Instruments). Quantitative bulk analysis was performed using SEMQuant program.

The thermal behaviour of the amorphous precursors from the HA and ZA systems was also examined by differential thermal analysis (DTA). The prepared samples were heated in the air atmosphere up to 950 °C with a rate of 10 °C min^{-1}, using the standard instrumentation.

3. Results and discussion

3.1. Thermal behaviour

Fig. 1 shows DTA curves of the samples from the HA and ZA systems with $AlO_{1.5}$ content between 0 and 60 mol%. All curves are characterized by endothermic peaks resulting from dehydration and exothermic peaks resulting from crystallization. The position of the exothermic peak shifted to the higher temperature with increasing Al^{3+} content. The crystallization temperature increased from 530 to 940 °C for the

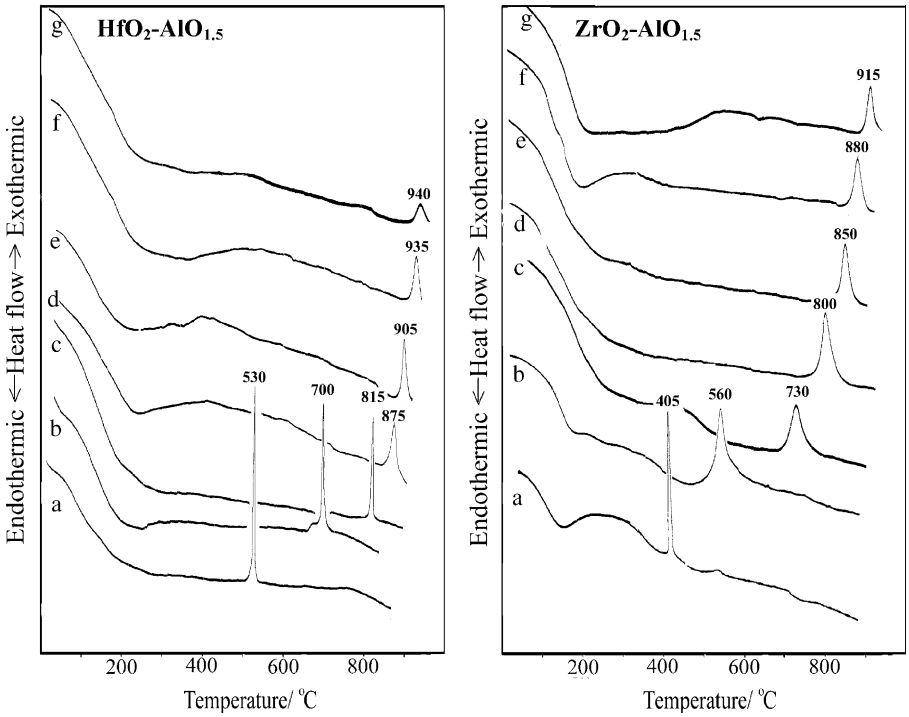

Fig. 1. DTA curves of the samples from HfO_2–$AlO_{1.5}$ and ZrO_2–$AlO_{1.5}$ systems. Letters a, b, c, d, e, f and g stand for 0, 10, 20, 30, 40, 50 and 60 mol% of $AlO_{1.5}$, respectively.

HA system and from 405 to 915 °C for ZA system. Similar results were observed for the HfO_2–$FeO_{1.5}$ and ZrO_2–$FeO_{1.5}$ systems [8], but in these cases, the rate of the increase was significantly smaller (Fig. 2). The observed increase indicated that amorphous precursors are single co-gels, which crystallized into metastable crystalline phases with extended capability for the formation of the solid solutions.

3.2. Phase analysis

Phase development of the amorphous precursors of the HfO_2–$AlO_{1.5}$ and ZrO_2–$AlO_{1.5}$ systems after calcinations (3 h) and cooling in the presence of air at atmospheric pressure are given in Table 1 . Amorphous precursors to the pure hafnia crystallized to *m*-HfO_2. The incorporation of Al^{3+} ions caused the appearance of the high-temperature tetragonal polymorph, which in the crystallization product of the samples with 20 and 30 mol% became the only phase present. However, the stabilization is not very efficient. Additional temperature treatment caused transition to the monoclinic polymorph and the appearance of aluminium oxide-type solid solutions (Table 1).

Differently form hafnia, the crystallization product obtained after calcinations of the amorphous precursor to pure zirconia contained *t*-ZrO_2 as the dominant phase with only traces of the thermodynamically stable *m*-ZrO_2 phase. Such a high content of metastable tetragonal polymorph can be attributed to the influence of grinding [3]. Further temperature treatment caused *t*-ZrO_2 → *m*-ZrO_2 transition, so that after treatment at 1000 °C, only traces of the metastable phase are still present (Fig. 3). The stability of the high-temperature polymorph of zirconia with regard to the influence of temperature increased with increasing of aluminium content and showed to be significantly bigger compared to the stability of corresponding high-temperature polymorphs of hafnia (Fig. 4). In some cases, it was hard to distinguished between the tetragonal and cubic polymorph of zirconia and almost impossible to distinguished between the tetragonal and cubic polymorph of hafnia, for which the c_f/a_f ratios approach 1 (a_f and c_f are related to fluorite-type lattice), on the basis of XRD analysis alone. In a series of papers, Yoshimura et al. [39–42] proved the existence of the tetragonal polymorph of hafnia with an axial ratio $c_f/a_f = 1$, having a displacement of the oxygen sublattice from the ideal fluorite positions. Due to the significantly smaller atomic scattering factor of oxygen compared to hafnium, X-ray diffraction is not very sensitive to structural changes caused by oxygen displacement. Laser Raman spectroscopy showed to be the most powerful technique in such cases [2,3,8,39–42]. Group theory allows six Raman active modes of vibration ($A_{1g} + 2B_{1g} + 3E_g$) for the tetragonal polymorph of zirconia and hafnia and only one active modes of vibration for their cubic polymorph (F_{2g}). All those six Raman active modes of vibration are present in the laser Raman spectra of the HA crystallization products with 20, 30 and 40 mol% of Al^{3+} ions and the spectra of the ZA crystallization products with 10, 40 and 50 mol% of Al^{3+} ions. The spectrum of the HA crystallization product with 40 mol% of Al^{3+} ions contained also small bands typ-

Table 1
The initial molar compositions and the results of phase analysis obtained after the calcination (3 h) and cooling of the amorphous precursors of the HfO_2–$AlO_{1.5}$ and ZrO_2–$AlO_{1.5}$ systems in the presence of air at atmospheric pressure

Molar fraction of $AlO_{1.5}$	T (°C)	Phase composition (relative volume fraction)	
		HfO_2–$AlO_{1.5}$ system	ZrO_2–$AlO_{1.5}$ system
–	400	Amorphous	*t*-ZrO_2 (0.98) + *m*-ZrO_2 (0.02)
	600	*m*-HfO_2	*m*-ZrO_2 (0.63) + *t*-ZrO_2 (0.37)
	800	*m*-HfO_2	*m*-ZrO_2 (0.85) + *t*-ZrO_2 (0.15)
	1000	*m*-HfO_2	*m*-ZrO_2 (0.97) + *t*-ZrO_2 (0.03)
	1300	*m*-HfO_2	*m*-ZrO_2
0.05	400	Amorphous	Amorphous
	500	H_m (0.87) + H_t (0.13)	Z_t
	600	H_m (0.92) + H_t (0.08)	Z_t
	800	H_m	Z_t (0.84) + Z_m (0.16)
	1000	H_m	Z_m (0.82) + Z_t (0.18)
	1100	H_m	Z_m (0.98) + Z_t (0.02)
	1300	H_m + A_α	Z_m + A_α
0.10	400	Amorphous	Amorphous
	600	H_t	Z_t
	800	H_m (0.70) + H_t (0.30)	Z_t (0.96) + Z_m (0.04)
	1000	H_m (0.99) + H_t (0.01)	Z_t (0.57) + Z_m (0.43)
	1100	H_m	Z_m (0.94) + Z_t (0.06)
	1300	H_m + A_α	Z_m + A_α
0.20	500	Amorphous	Amorphous
	600	Amorphous	Amorphous + Z_t
	700	Amorphous + H_t	Z_t
	800	H_t	Z_t
	1000	H_m (0.98) + H_t (0.02)	Z_t
	1100	H_m + A_α	Z_m (0.92) + Z_t (0.08) + A_δ + A_α
	1300	H_m + A_α	Z_m + A_α + Z_t
0.30	700	Amorphous	–
	800	H_t	Z_t
	1000	H_m (0.98) + H_t (0.02)	Z_t
	1100	H_m + A_α	Z_m (0.85) + Z_t(0.15) + A_δ + A_α
	1300	H_m + A_α + H_t	Z_m (0.98) + Z_t (0.02) + A_α
0.40	700	–	Amorphous
	800	Amorphous + H_t	Z_t
	900	H_t + H_m	–
	1000	H_m + H_t + A_δ	Z_t
	1100	H_m + H_t + A_α + A_δ	Z_t + Z_m + A_δ + A_α
	1300	H_m + A_α + H_t	Z_m + Z_t + A_α
0.50	700	–	Amorphous
	800	Amorphous + H_t	Z_t
	900	H_t + H_m + A_δ	–
	1000	H_m + H_t + A_δ + A_α	Z_t + A_δ
	1100	H_m + H_t + A_α + A_δ	Z_t + A_δ + A_α
	1300	H_m + H_t + A_α + A_δ	Z_m + Z_t + A_α
0.60	800	Amorphous + H_t	Amorphous + Z_t
	900	–	Z_t + A_δ
	1000	H_t + H_m + A_δ	Z_t + A_δ
	1100	H_m + H_t + A_δ + A_α	Z_t + A_δ + A_α
	1300	A_α + H_m	A_α + Z_m + Z_t
0.70	800	Amorphous	Amorphous + Z_t
	1000	H_t + H_m + A_δ	A_δ + Z_t
	1100	A_δ + A_α + H_m + H_t	A_δ + A_α + Z_t
	1300	A_α + H_m + H_t	A_α + Z_m + Z_t
0.80	800	Amorphous	Amorphous + Z_t
	900	–	A_γ + Z_t
	1000	H_t + H_m + A_δ	A_δ + Z_t
	1100	A_δ + A_α + H_m	A_α + A_a + Z_t
	1300	A_α + H_m	A_α + Z_m + Z_t

Table 1 (*Continued*)

Molar fraction of $AlO_{1.5}$	T (°C)	Phase composition (relative volume fraction)	
		HfO_2–$AlO_{1.5}$ system	ZrO_2–$AlO_{1.5}$ system
0.90	–	–	Amorphous
	800	Amorphous	Amorphous + A_γ or A_δ
	1000	$A_\delta + A_\alpha + H_t + H_m$	$A_\delta + Z_t$
	1100	$A_\delta + A_\alpha + H_m + H_t$	$A_\delta + A_\alpha + Z_t + Z_m$
	1300	$A_\alpha + A_\delta + H_m + H_t$	$A_\alpha + Z_t + Z_m$
0.95	–	Amorphous	$A_\gamma + A_\delta$
	400	–	Amorphous + A_γ
	600	–	Amorphous + A_γ
	1000	Amorphous + $A_\delta + H_m + H_t$	Amorphous + $A_\delta + Z_t$
	1100	$Z_t + A$	$A_\alpha + A_\delta + Z_t + Z_m$
	1300	$Z_t + A$	$A_\alpha + Z_m + Z_t$
1.00	–	Amorphous	A_B
	600	–	A_γ
	800	A_γ	A_δ
	1000	$A_\delta + A_\alpha$	$A_\delta + A_\alpha$
	1100	$A_\alpha + A_\delta$	$A_\alpha + A_\delta$
	1300	A_α	A_δ

Description: The symbols Z_m, Z_t, H_m, H_t, A_B, A_G, A_α, A_γ, A_δ stand for the phases structurally similar to *m*-ZrO_2, *t*-ZrO_2, *m*-HfO_2, *t*-HfO_2, beohmite, gibbsite, α-Al_2O_3, γ-Al_2O_3 and δ-Al_2O_3, respectively.

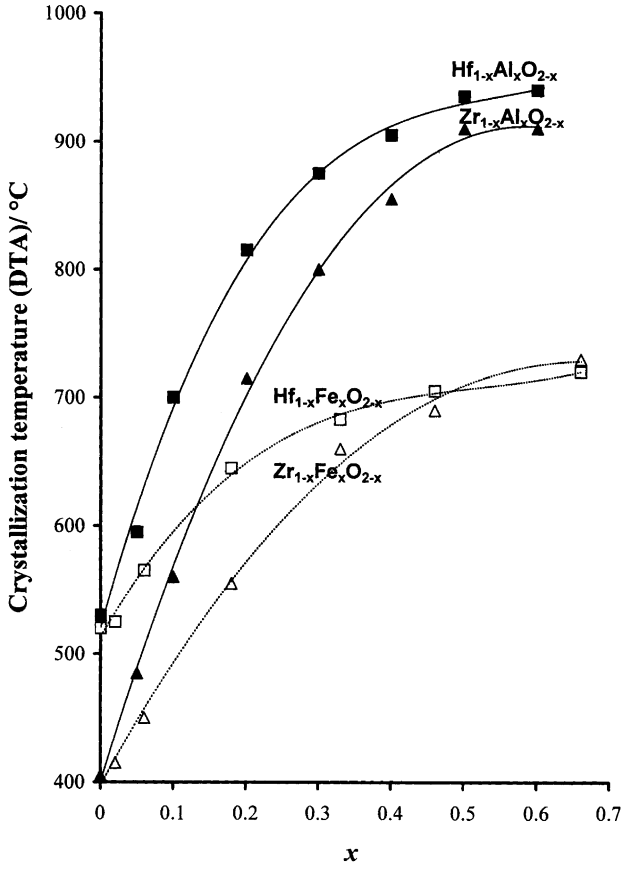

Fig. 2. The influence of the molar fraction of $AlO_{1.5}$ and $FeO_{1.5}$ on the crystallization temperatures of the amorphous precursors of HfO_2–$AlO_{1.5}$ (full square), HfO_2–$FeO_{1.5}$ (empty square), ZrO_2–$AlO_{1.5}$ (full triangle) and ZrO_2–$FeO_{1.5}$ (empty triangle) systems.

ical of monoclinic polymorph (Fig. 5). These results show that regardless to the amount of Al^{3+} ions only tetragonal polymorph of HfO_2 and ZrO_2 could be stabilized.

On the Al-rich side of the concentration range, besides the ZrO_2 and HfO_2-type solid solutions, the crystallization products contained aluminium oxide-type solid solutions. The solubility of Zr^{4+} or Hf^{4+} ions in the lattice of the aluminium oxides appeared to be very small (less than 5 mol%). Due to that, phase developments during the temperature treatment of aluminium oxide-type solid solutions are not very different from the phase development of pure aluminium oxide. However, the phase transitions on calcinations occurred at somewhat higher temperatures. The starting material obtained after precipitation from the aqueous solution of $Al(NO_3)_3$ was characterized as γ-AlOOH, which, on calcination, underwent phase transitions, first to γ-Al_2O_3, then to δ-Al_2O_3 and finally to α-Al_2O_3. The amorphous phase, obtained after precipitation from an aqueous solution of $AlCl_3$, crystallized on calcination to γ-Al_2O_3, which underwent phase transitions to δ-Al_2O_3 and finally to α-Al_2O_3.

3.3. Lattice parameters

Precise determinations of the unit-cell parameters of the HfO_2- and ZrO_2-type solid solutions were performed using the whole-powder-pattern decomposition method (WPPF program, [38]), following the procedure described previously [8]. The fitting was performed in the scanned 2θ range, from 20° to 110°, using the split-type pseudo-Voigt profile function and the polynomial background model. Figs. 6 and 7 show the observed and calculated powder patterns of the crystallization products from the HA and ZA series, respectively. Although laser Raman spectroscopy indicated that, regardless

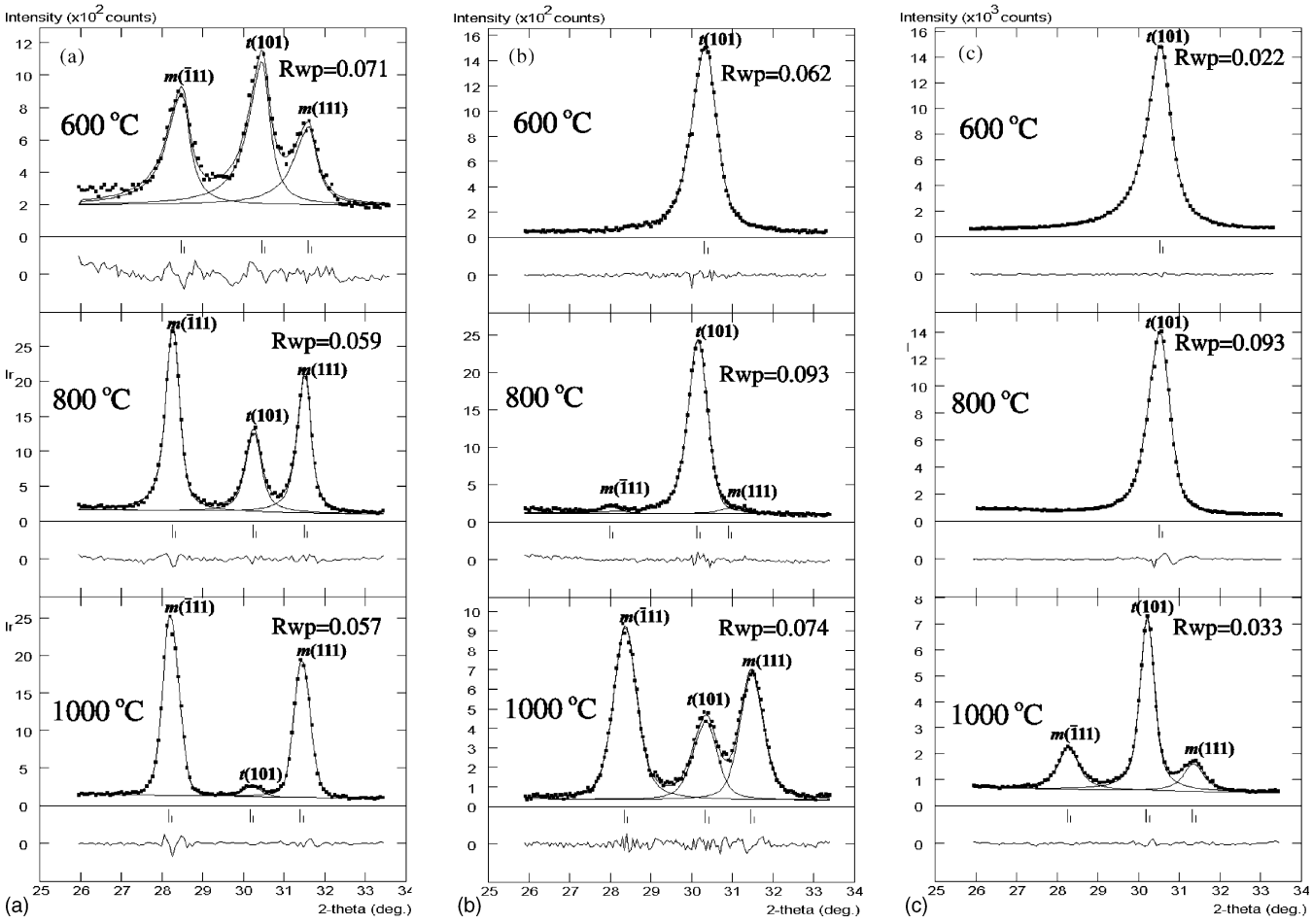

Fig. 3. Individual profile-fitting results of the crystallization products from ZrO_2–$AlO_{1.5}$ system with 0 mol% of $AlO_{1.5}$ (a), 5 mol% of $AlO_{1.5}$ (b) and 10 mol% of $AlO_{1.5}$ (c). Observed data are represented by squares, and the calculated one by full line. Long and short vertical bars marked the Cu $K\alpha_1$ and Cu $K\alpha_2$ positions of the reflection, respectively. Differences between the observed and calculated intensities are plotted in the same scale below.

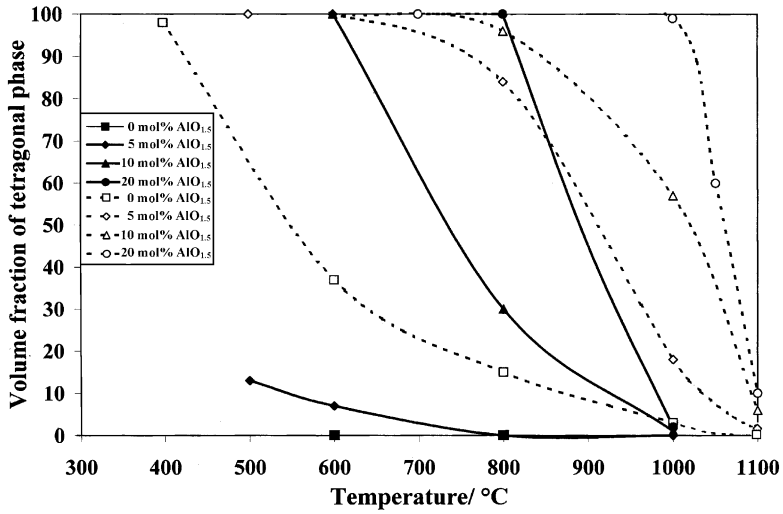

Fig. 4. Volume fraction of tetragonal polymorphs of HfO_2 (full line) and ZrO_2 (broken line) in the product obtained after 3 h of calcinations of the amorphous precursors of the HfO_2–$AlO_{1.5}$ and ZrO_2–$AlO_{1.5}$ systems at the selected temperatures.

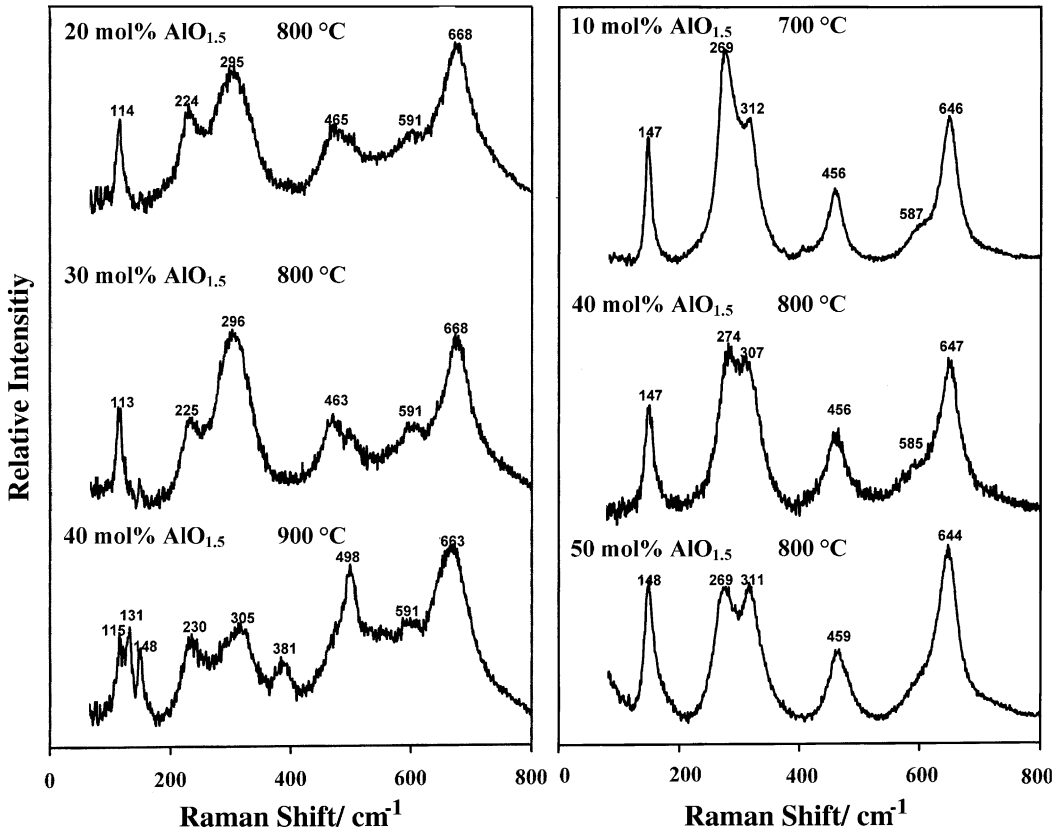

Fig. 5. Laser Raman spectra of the crystallization products from the HfO_2–$AlO_{1.5}$ system (left) and ZrO_2–$AlO_{1.5}$ system (right).

the amount of the incorporated Al^{3+} ions, only the tetragonal polymorph of hafnia and zirconia can be stabilized, the results of WPPF showed that the axial ratios c_f/a_f in the crystallization products with 10 or more mol% of Al^{3+} approach 1 (Table 3). The tetragonal symmetry of these samples can be explained by the displacement of oxygen sublattice [39–42]. In case of the system ZA, the obtained results indicate a decrease of the lattice parameters with increasing Al^{3+} content up to ~10 mol%. An additional increase of the Al^{3+} content has a very small influence on the lattice parameters. A similar result was obtained for the HA system with 10–40 mol% of Al^{3+} (Table 3).

In accordance with Vegard's law Kim et al. [10,11] proposed empirical equations that relate the lattice constants of the fluorite-type HfO_2 and ZrO_2 solid solutions with the type (ionic radius, valency) and concentration of the dopant cations. For the HfO_2–$RO_{1.5}$ and ZrO_2–$RO_{1.5}$ systems, these equations can be expressed as follows:

$$\frac{a_{Hf}}{nm} = 0.5098 + (0.0203\,\Delta r - 0.00022)m \quad (4)$$

$$\frac{a_{Zr}}{nm} = 0.5120 + (0.0212\,\Delta r - 0.00023)m \quad (5)$$

where a_{Hf} and a_{Zr} are lattice constants of the *c*-HfO_2- and *c*-ZrO_2-type solid solutions, respectively, Δr is the difference in ionic radius of dopant cation (R^{3+}) and the host cation (Hf^{4+} or Zr^{4+}), and *m* is the concentration of the dopant cation (mol%) in the form of $RO_{1.5}$. These empirical relations were developed from the lattice parameters obtained from the HfO_2- and ZrO_2-type solid solutions with divalent or trivalent oversized dopant cations. The results presented here, as well as our previous results obtained for the HfO_2–$FeO_{1.5}$ and ZrO_2–$FeO_{1.5}$ systems [8], showed that these equations could not be used in cases of HfO_2 and ZrO_2 solid solutions with dopant cations significantly smaller than Hf^{4+} (0.83 Å, [43]) or Zr^{4+} (0.84 Å, [43]) ions. The incorporation of Fe^{3+} ions (0.65 Å, [43]) caused a linear decrease of the lattice parameters of HfO_2- and ZrO_2-type solid solution, but the rate of the decrease is about two times smaller than it should be according to the relations above (Fig. 8). In the case of the ZrO_2–$FeO_{1.5}$ system, a smaller amount of Fe^{3+} ions stabilized the tetragonal polymorph. However, the unit-cell volume of these samples showed to be on the same line, which indicates that the transition from a tetragonal to a cubic polymorph has a very small influence on the unit-cell volume. In case of the ZrO_2–$AlO_{1.5}$ system the increase of the Al^{3+} ion (0.54 Å, [43]) content up to 10 mol% caused a decrease of the unit-cell volume. The rate of the decrease is bigger than for the ZrO_2–$FeO_{1.5}$ system, but smaller than it should be according to the relations proposed by Kim et al. [10,11]. However, in the concentration range between 10 and 50 mol% of Al^{3+} ions, the increase of the Al^{3+} content had very small influence

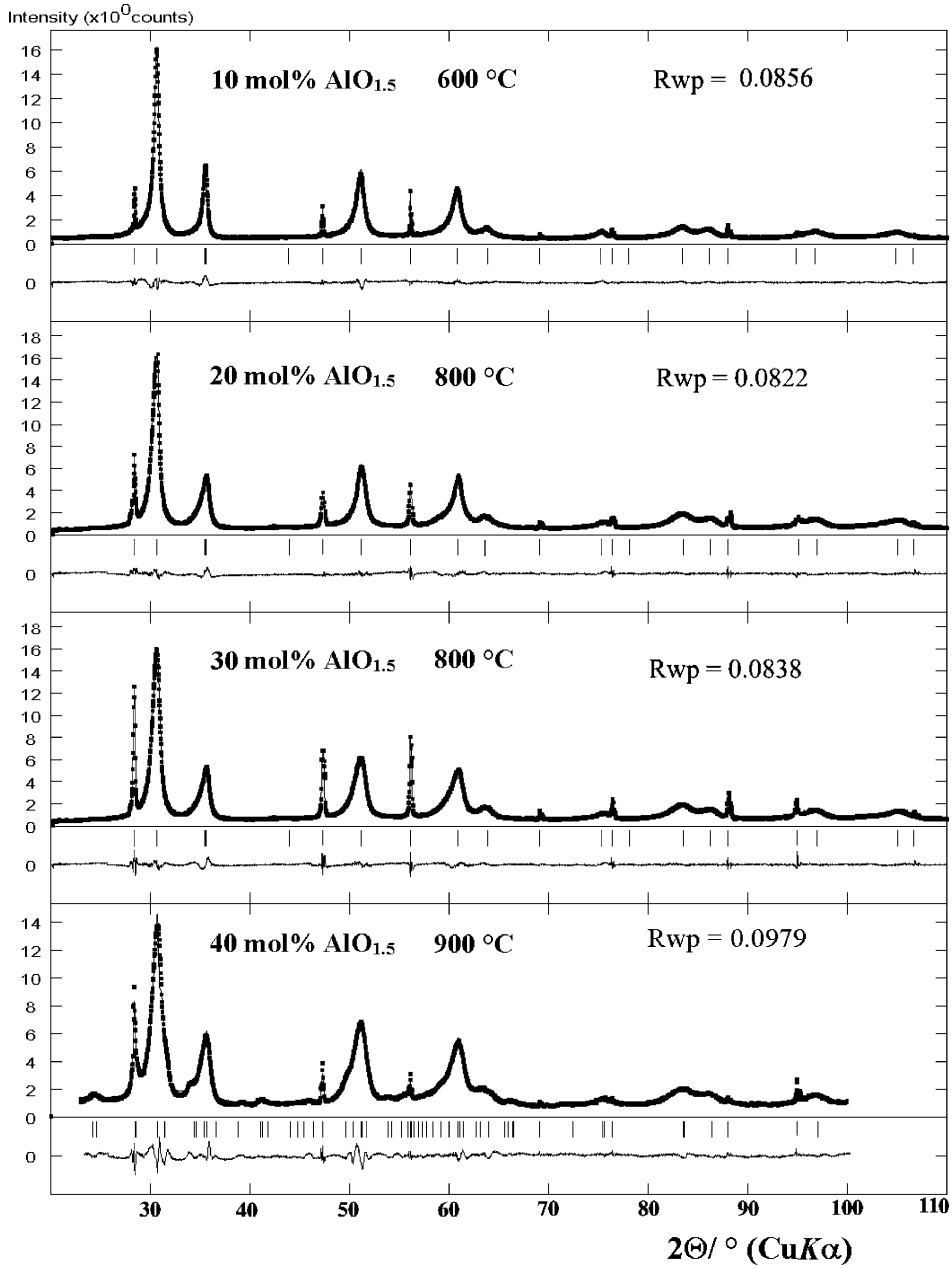

Fig. 6. Whole-powder-pattern decomposition results for the crystallization products from the HfO_2–$AlO_{1.5}$ system and Si as internal standard. Observed data are shown by squares, the calculated one by full line. Short and long vertical bars marked the Bragg reflection positions of the crystallization products and standard, respectively. The differences between the observed and calculated intensities are plotted in the same scale below each pattern.

on the unit-cell volume of the *t*-HfO_2- and *t*-ZrO_2-type solid solutions (Fig. 8). These results cannot be explained by standard model of cation substitution and random distribution of oxygen vacancies.

3.4. The solubility of Al^{3+} ions

No sign of the diffraction lines of aluminium oxide phases in the XRD patterns of HA and ZA crystallization products with 50 mol% of aluminium indicates very high solubility of Al^{3+} ions. High solubility was also indicated by the results of SEM/EDX analysis. SEM images of the crystallization product, obtained after calcination of the amorphous precursors from ZA system with 10, 40 and 50 mol% of Al^{3+} ions at 800 °C, show only one type of grains (Fig. 9). The results of quantitative analysis (Table 2) showed to be in good agreement with initial molar fraction of the samples. The aluminium distribution showed to be uniform in the whole area of the image, which also indicated the formation of the solid solution. However, precise measurement of unit-cell parameters shows that an increase of the aluminium fraction above 10 mol% has very small influence on the unit-cell volume of the HfO_2- or ZrO_2-type solid solutions (Fig. 8). Such results are hard to explain when we consider the significantly smaller

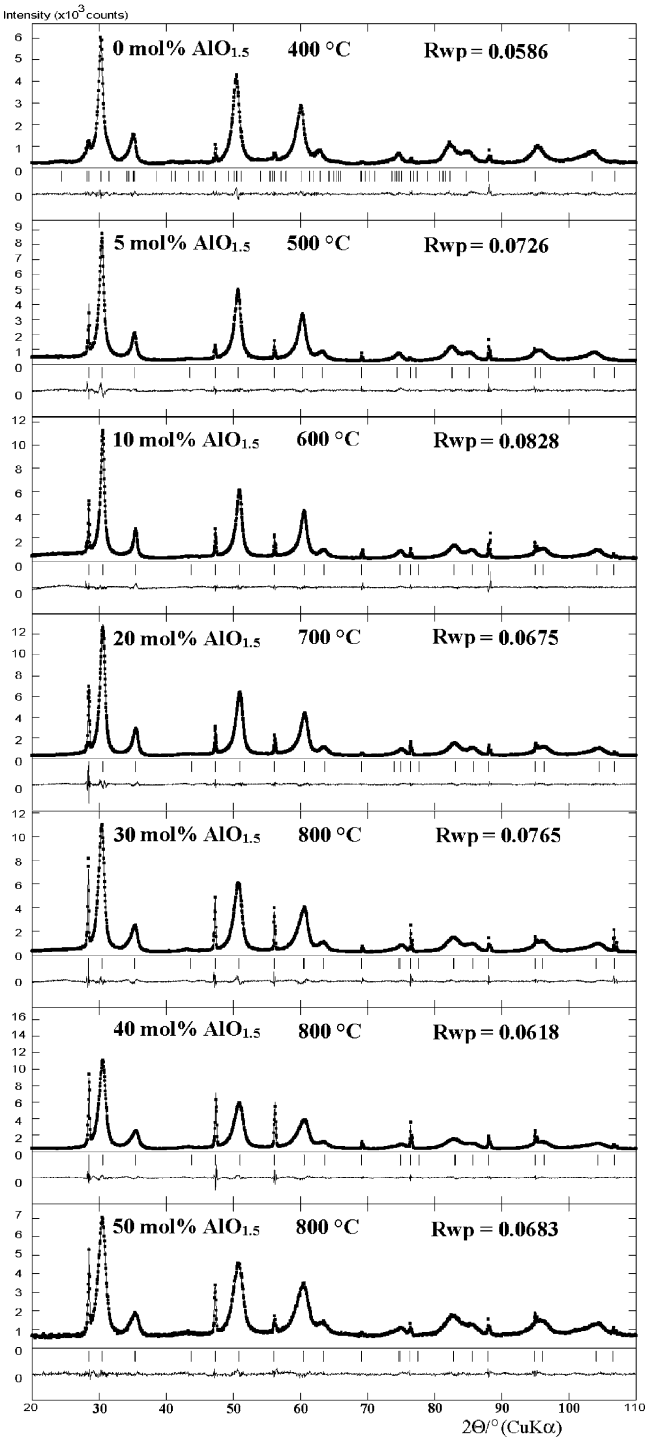

Fig. 7. Whole-powder-pattern decomposition results for the crystallization products from the ZrO_2–$AlO_{1.5}$ system and Si as internal standard. Observed data are shown by squares, the calculated one by full line. Short and long vertical bars marked the Bragg reflection positions of the crystallization products and standard, respectively. Differences between the observed and calculated intensities are plotted in the same scale below each pattern.

Table 2
Refined values of unit-cell parameters of the *t*-HfO_2- and *t*-ZrO_2-type solid solutions with different amount of incorporated Al^{3+} ions

Phase	*a* (Å)	*c* (Å)	*V* (Å^3)	R_{wp}
t-$Hf_{0.90}Al_{0.10}O_{1.95}$	3.5682 (8) 5.0462 (11)[a]	5.0451 (14)	64.23 (5) 128.47 (8)[a]	0.0855
t-$Hf_{0.80}Al_{0.20}O_{1.90}$	3.5643 (8) 5.0407 (11)[a]	5.0360 (13)	63.98 (5) 127.96 (7)[a]	0.0823
t-$Hf_{0.70}Al_{0.30}O_{1.85}$	3.5661 (8) 5.0441 (11)[a]	5.0388 (14)	64.08 (5) 128.18 (8)[a]	0.0838
t-$Hf_{0.60}Al_{0.40}O_{1.80}$	3.5634 (8) 5.0394 (11)[a]	5.0293 (14)	63.87 (5) 127.74 (8)[a]	0.0979
t-ZrO_2	3.6057 (6) 5.0992 (8)[a]	5.1475 (14)	66.92 (4) 133.85 (7)[a]	0.0586
t-$Zr_{0.95}Al_{0.05}O_{1.98}$	3.5974 (5) 5.0875 (8)[a]	5.0918 (9)	65.89 (3) 131.79 (5)[a]	0.0726
t-$Zr_{0.90}Al_{0.10}O_{1.95}$	3.5858 (5) 5.0711 (7)[a]	5.0691 (8)	65.18 (3) 130.36 (5)[a]	0.0828
t-$Zr_{0.80}Al_{0.20}O_{1.90}$	3.5832 (4) 5.0674 (6)[a]	5.0643 (6)	65.00 (2) 129.99 (4)[a]	0.0675
t-$Zr_{0.70}Al_{0.30}O_{1.85}$	3.5904 (6) 5.0776 (8)[a]	5.0672 (9)	65.32 (3) 130.64 (5)[a]	0.0765
t-$Zr_{0.60}Al_{0.40}O_{1.80}$	3.5835 (5) 5.0678 (7)[a]	5.0637 (8)	65.03 (3) 130.05 (5)[a]	0.0618
t-$Zr_{0.50}Al_{0.50}O_{1.75}$	3.5816 (4) 5.0651[a]	5.0643 (5)	64.964 129.93[a]	0.0683

[a] Related to fluorite-type lattice.

radius of Al^{3+} ion (0.54 Å) compared to the radii of Hf^{4+} (0.83 Å) and Zr^{4+} (0.84 Å) ions [43]. Here, we would like to pay attention to the publication of Balmer et al. [34]. The authors used ^{27}Al NMR to investigate local environment of aluminium atoms in a series of metastable $Zr_{1-x}Al_xO_{2-x/2}$ crystalline materials with Al^{3+} content up to 57 mol%. The obtained results showed that the products with Al_2O_3 content above 10 mol% contain Al^{3+} ions in four-fold coordination, which cannot be explained by the standard model of cation substitution in the solid solutions. The authors proposed two possible explanations of these results. The first one associated the four-fold coordinated aluminium with a

Table 3
The results of EDX analysis (program SEMQuant) of the crystallization product from ZrO_2–$AlO_{1.5}$ system with 10, 40 and 50 mol% of Al^{3+} ions calcinated at 800 °C

Initial Al/Zr ratio	Element	At.%	Obtained Al/Zr ratio
0.11	O	73.01	0.09
	Al	2.30	
	Zr	24.69	
0.67	O	70.88	0.64
	Al	11.41	
	Zr	17.71	
1.00	O	69.90	0.99
	Al	15.02	
	Zr	15.08	

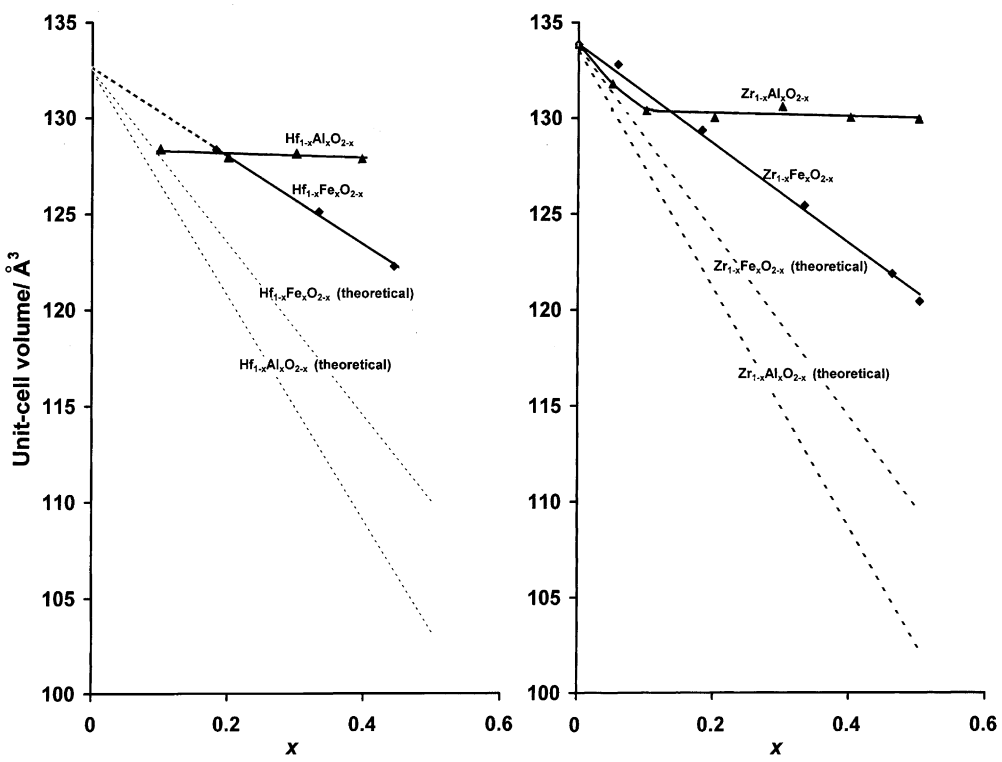

Fig. 8. Influence of the dopant cations (Al^{3+} or Fe^{3+}) content on the unit cell-volume of the corresponding fluorite-type HfO_2 and ZrO_2 solid solutions. Dash lines represent theoretical values calculated from the empirical relations proposed by Kim et al. [10,11].

residual amorphous phase, present in the samples due to the incomplete crystallization. The second explanation assumed the existence of aluminium-rich clusters as disordered regions within the individual crystallites or on their surfaces. The authors concluded that solid solutions with random distributions of oxygen vacancies exist only in the products with molar fractions of aluminium below 10 mol% [34]. This conclusion is in good agreement with our results obtained

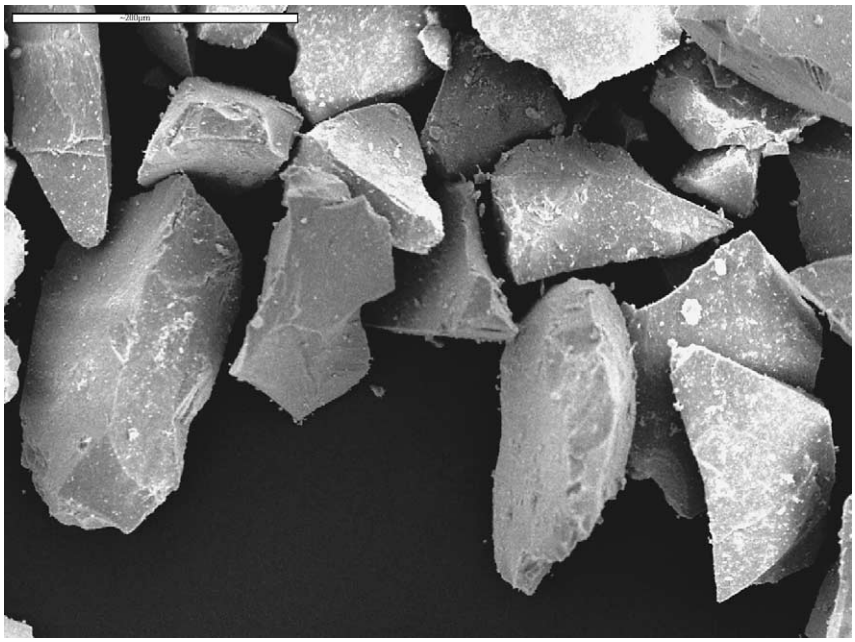

Fig. 9. SEM image of the crystallization products from the ZrO_2–$AlO_{1.5}$ system with 50 mol% of $AlO_{1.5}$, obtained after 3 h of calcination at 800 °C in the air atmosphere and cooling to room temperature.

from the measurements of the unit-cell volume. In case of the products with molar fraction of aluminium above 10 mol%, the second explanation proposed by Balmer et al. [34] seems to be more realistic. SEM images of the crystallization product with a ratio Zr/Al = 1 indicate the presence of only one type of grains. No sign of the significant amount of amorphous phase, required to compensate the difference in the aluminium content between 10 and 50 mol% could be found.

4. Conclusion

The results of the DTA showed that the crystallization temperature of the amorphous precursors of the HfO_2–$AlO_{1.5}$ and ZrO_2–$AlO_{1.5}$ systems increased with increasing $AlO_{1.5}$ content, from 530 °C (0 mol% $AlO_{1.5}$) to 940 °C (60 mol% $AlO_{1.5}$) and from 405 °C (0 mol% $AlO_{1.5}$ to 915 °C (60 mol% $AlO_{1.5}$), respectively. These results indicated that in this concentration range amorphous precursors exist in the form of a co-gel. The results of phase analysis obtained using XRD, laser Raman spectroscopy and SEM/EDX showed only the presence of HfO_2- and ZrO_2-type solid solutions in the crystallization products with $AlO_{1.5}$ contents $\leq$50 mol%. These results suggested an extended capability for the formation of solid solutions in these metastable phases. However, precise measurement of unit-cell parameters shows that an increase of the aluminium content above 10 mol% has a very small influence on the unit-cell volume of the HfO_2- or ZrO_2-type solid solutions. Such results could not be explained by the standard model of cation substitution and random distribution of oxygen vacancies due to the significantly smaller radius of Al^{3+} ion (0.54 Å) compared to the radii of Hf^{4+} (0.83 Å) and Zr^{4+} (0.84 Å) ions. It was concluded that solid solutions with random distributions of oxygen vacancies exist only in the products with molar fractions of aluminium below 10 mol%. In case of the products with molar fractions of aluminium above 10 mol%, the model proposed by Balmer et al. [34], which assume the existence of aluminium-rich clusters as disordered regions within the individual crystallites or on their surfaces, seems to be the most realistic. The appearance of such clusters in the products with aluminium contents above 10 mol% is probably the reason why only the tetragonal polymorph of hafnia and zirconia could be stabilized. Although the results of whole-powder-pattern decomposition indicated stabilization of the cubic polymorphs of HfO_2 and ZrO_2 in the products with $AlO_{1.5}$ content $\geq$10 mol% (axial ratio c_f/a_f approach (1), Raman spectra of those crystallization products contained all six Raman active modes of vibration, typical for the tetragonal polymorphs of HfO_2 and ZrO_2. The tetragonal symmetry of these samples can be attributed to the displacement of oxygen sub-lattice from the ideal fluorite positions. On the other side of the concentration range the solubility of Zr^{4+} and Hf^{4+} ions in the aluminium oxides lattice appeared to be negligible.

References

[1] I. Clark, D.H. Reynolds, Ind. Eng. Chem. 29 (1937) 711–715.
[2] G. Štefanić, S. Musić, Croat. Chem. Acta 75 (2002) 727–767.
[3] G. Štefanić, S. Musić, S. Sekulić, Thermochim. Acta 273 (1996) 119–133.
[4] A. Larbot, T. Hours, P. Bergez, J. Charpin, L. Cot, J. Non-Cryst. Solids 147/148 (1992) 85–91.
[5] L.-M. Tau, R. Srinivasan, R.J. De Angelis, T. Pinder, B.H. Davis, J. Mater. Res. 3 (3) (1988) 561–562.
[6] R. Srinivasan, B.H. Davis, J. Am. Ceram. Soc. 73 (6) (1990) 1780–1782.
[7] G. Štefanić, S. Musić, Thermochim. Acta 373 (2001) 59–67.
[8] G. Štefanić, B. Gržeta, K. Nomura, R. Trojko, S. Musić, J. Alloys Compd. 327 (2001) 151–160.
[9] S.M. Ho, Mater. Sci. Eng. 54 (1982) 23–29.
[10] D.-J. Kim, J. Am. Ceram. Soc. 72 (1989) 1415–1421.
[11] D.-J. Kim, S.-H. Hyun, S.-G. Kim, M. Yashima, J. Am. Ceram. Soc. 77 (1994) 597–599.
[12] M. Yashima, H. Takahashi, K. Ohtake, T. Hirose, M. Kakihana, H. Arashi, Y. Ikuma, Y. Suzuki, M. Yoshimura, J. Phys. Chem. Solids 157 (1996) 289–295.
[13] M. Yashima, N. Ishizawa, M. Yoshimura, J. Am. Ceram. Soc. 75 (1992) 1541.
[14] M.F. Trubelja, V.S. Stubican, Solid State Ionics 49 (1991) 89–97.
[15] V.V. Kharton, A.A. Yaremchenko, E.N. Naumovich, F.M.B. Marques, J. Solid State Electrochem. 4 (2000) 243–266.
[16] C.J. Howard, R.J. Hill, B.E. Reichert, Acta Crystallogr. Sect. B 44 (1988) 116–120.
[17] P. Li, I.-W. Chen, J.E. Penner-Hahn, J. Am. Ceram. Soc. 77 (1994) 118–128.
[18] S. Popović, B. Gržeta, G. Štefanić, I. Cakó-Nagy, S. Musić, J. Alloys Compd. 241 (1996) 10–15.
[19] S. Popović, G. Štefanić, S. Musić, Mater. Lett. 31 (1997) 19–22.
[20] G. Štefanić, S. Popović, S. Musić, Mater. Lett. 36 (1998) 240–244.
[21] S. Davison, R. Kershaw, K. Dwight, A. Wold, J. Solid State Chem. 73 (1988) 47–51.
[22] F.J. Berry, M.H. Loretto, M.R. Smith, J. Solid State Chem. 83 (1989) 91–99.
[23] I.B. Inwang, F. Chyad, I.J. McColm, J. Mater. Chem. 5 (1995) 1209–1213.
[24] G. Štefanić, B. Gržeta, S. Musić, Mater. Chem. Phys. 65 (2000) 216.
[25] O. Yamaguchi, M. Shirai, M. Yoshinaka, J. Am. Ceram. Soc. 71 (1988) C-510–C-512.
[26] K. Ishida, K. Hirota, O. Yamaguchi, H. Kume, S. Inamura, H. Miyamoto, J. Am. Ceram. Soc. (1994) 77.
[27] W. Zhang, E.E. lachowski, F.P. Glasser, J. Mater. Sci. 28 (1993) 6222–6232.
[28] J.S. Hong, S.D. De la Torre, K. Miyamoto, H. Miyamoto, L. Gao, Mater. Lett. 37 (1998) 6–9.
[29] A. Mondal, S. Ram, Solid State Ionics 160 (2003) 169–181.
[30] S. Kikkawa, A. Kijima, K. Hirota, O. Yamamoto, J. Am. Ceram. Soc. 85 (2002) 721–723.
[31] S. Moreau, M. Gervais, A. Douy, Solid State Ionics 101–103 (1997) 625–631.
[32] M.L. Balmer, F.F. Lange, C.G. Levi, J. Am. Ceram. Soc. 77 (1994) 2069–2075.
[33] M.L. Balmer, F.F. Lange, V. Jayaram, C.G. Levi, J. Am. Ceram. Soc. 78 (1995) 1489–1494.
[34] M.L. Balmer, H. Eckert, N. Das, F.F. Lange, J. Am. Ceram. Soc. 79 (1996) 321–326.
[35] M. Yoshimura, S.-T. Oh, M. Sando, K. Niihara, J. Alloys Compd. 290 (1999) 284–289.

[36] Powder Diffraction File, International Center for Diffraction Data, Newtown Square, PA 19073-3273, USA.
[37] H. Toraya, M. Yoshimura, S. Somiya, J. Am. Ceram. Soc. 67 (1984) C119–C121.
[38] H. Toraya, J. Appl. Cryst. 19 (1986) 440–447.
[39] M. Yashima, T. Hirose, M. Kakihana, Y. Suzuki, M. Yoshimura, J. Ceram. Soc. Jpn. Int. Ed. 103 (1995) 622–628.
[40] H. Fujimori, M. Yashima, S. Sasaki, M. Kakihana, T. Mori, M. Tanaka, M. Yoshimura, Chem. Phys. Lett. 346 (2001) 217–223.
[41] H. Fujimori, M. Yashima, S. Sasaki, M. Kakihana, T. Mori, M. Tanaka, M. Yoshimura, Phys. Rev. B 64 (13) (2001) 41041–41045.
[42] H. Fujimori, M. Yashima, M. Kakihana, M. Yoshimura, J. Am. Ceram. Soc. 84 (2001) 663–665.
[43] R.D. Shannon, Acta Cryst. A 32 (1976) 751–767.